

# Lurbinectedin Inactivates the Ewing Sarcoma Oncoprotein EWS-FLI1 by Redistributing It within the Nucleus

Matt L. Harlow<sup>1</sup>, Nichole Maloney<sup>2</sup>, Joseph Roland<sup>3</sup>, Maria Jose Guillen Navarro<sup>4</sup>, Matthew K. Easton<sup>5</sup>, Susan M. Kitchen-Goosen<sup>5</sup>, Elissa A. Boguslawski<sup>5</sup>, Zachary B. Madaj<sup>5</sup>, Ben K. Johnson<sup>5</sup>, Megan J. Bowman<sup>5</sup>, Maurizio D'Incalci<sup>6</sup>, Mary E. Winn<sup>5</sup>, Lisa Turner<sup>5</sup>, Galen Hostetter<sup>5</sup>, Carlos María Galmarini<sup>4</sup>, Pablo M. Aviles<sup>4</sup>, and Patrick J. Grohar<sup>2,5,7,8</sup>

## Abstract

There is a great need to develop novel approaches to target oncogenic transcription factors with small molecules. Ewing sarcoma is emblematic of this need, as it depends on the continued activity of the EWS-FLI1 transcription factor to maintain the malignant phenotype. We have previously shown that the small molecule trabectedin interferes with EWS-FLI1. Here, we report important mechanistic advances and a second-generation inhibitor to provide insight into the therapeutic targeting of EWS-FLI1. We discovered that trabectedin functionally inactivated EWS-FLI1 by redistributing the protein within the nucleus to the nucleolus. This effect was rooted in the wild-type functions of the EWSR1, compromising the N-terminal half of the chimeric oncoprotein, which is known to be similarly redistributed within the nucleus in

the presence of UV light damage. A second-generation trabectedin analogue lurbinectedin (PM01183) caused the same nuclear redistribution of EWS-FLI1, leading to a loss of activity at the promoter, mRNA, and protein levels of expression. Tumor xenograft studies confirmed this effect, and it was increased in combination with irinotecan, leading to tumor regression and replacement of Ewing sarcoma cells with benign fat cells. The net result of combined lurbinectedin and irinotecan treatment was a complete reversal of EWS-FLI1 activity and elimination of established tumors in 30% to 70% of mice after only 11 days of therapy. Our results illustrate the preclinical safety and efficacy of a disease-specific therapy targeting the central oncogenic driver in Ewing sarcoma. *Cancer Res*; 76(22); 6657–68. ©2016 AACR.

## Introduction

Ewing sarcoma is a bone and soft-tissue sarcoma that depends on the continued activity of the EWS-FLI1 transcription factor, which is formed by the t(11;22)(q24;q12) chromosomal translocation (1, 2). This translocation leads to the fusion of the binding domain of the ETS family member FLI1 to the transactivation domain of EWSR1 and the loss of negative regulatory domains. The result is a constitutively active transcription factor that both drives and suppresses the expression of more than 500 genes (3–5). Silencing of EWS-FLI1 activity is incompatible with continued proliferation and places the cell in a dedifferentiated state, which resembles that of mesenchymal stem cells (2, 6, 7). Therefore, a therapy directed against

EWS-FLI1 would be expected to block proliferation and potentially allow the tumor to differentiate into a benign tissue, such as fat. Unfortunately, because transcription factors are challenging drug targets, the successful suppression of EWS-FLI1 in the clinic has not been achieved.

In this report, we describe a novel method of targeting oncogenic fusion transcription factors with small molecules, a method likely applicable to a variety of tumors. For any fusion protein, there exists a competition between the wild-type functions of each fusion partner and the oncogenic properties that result when these proteins are joined. At baseline, the activity of the fusion protein dominates, and the protein subsequently functions as an oncogene. However, it is possible that the wild-type functions preserved in the fusion can be activated to overcome the oncogenic properties.

We apply this method in this study to target and functionally inactivate EWS-FLI1. To accomplish this, we leverage the wild-type properties of EWSR1 retained within the fusion protein to redistribute EWS-FLI1 in the nucleus. Wild-type EWSR1 is known to play an important role in RNA processing but has recently emerged as a key protein in the DNA damage response (DDR) to UV light by redistributing within the nucleus to the nucleolus (8). We have previously shown that treatment of Ewing sarcoma cells with trabectedin, a DNA-binding agent, generates a gene signature resembling that found after UV light treatment of keratinocytes (9). Therefore, we hypothesized that if this sequestration of EWSR1 was preserved in the EWS-FLI1 fusion protein, trabectedin treatment would remove the protein from its target sequences by moving it into the nucleolus.

<sup>1</sup>Department of Cancer Biology, Vanderbilt University, Nashville, Tennessee. <sup>2</sup>Department of Pediatrics, Vanderbilt University, Nashville, Tennessee. <sup>3</sup>Epithelial Biology Center, Vanderbilt University School of Medicine, Nashville, Tennessee. <sup>4</sup>PharmaMar, Madrid, Spain. <sup>5</sup>Van Andel Research Institute, Grand Rapids, Michigan. <sup>6</sup>IRCCS - Istituto di Ricerche Farmacologiche Mario Negri, Milan, Italy. <sup>7</sup>Helen De Vos Children's Hospital, Grand Rapids, Michigan. <sup>8</sup>Department of Pediatrics, Michigan State University, Grand Rapids, Michigan.

**Note:** Supplementary data for this article are available at Cancer Research Online (<http://cancerres.aacrjournals.org/>).

**Corresponding Author:** Patrick J. Grohar, Van Andel Institute, 333 Bostwick Ave NE, Grand Rapids, MI 49503. Phone: 616-234-5489; Fax: 616-234-5309; E-mail: [patrick.grohar@vai.org](mailto:patrick.grohar@vai.org)

**doi:** 10.1158/0008-5472.CAN-16-0568

©2016 American Association for Cancer Research.

We show here that activation of the UV light-induced DDR by trabectedin indeed led to the sequestration of EWS-FLI1 to the nucleolus. We show that a second-generation trabectedin analogue, lurbinectedin, which is known to accumulate at much higher serum levels in patients, accomplishes the same redistribution of EWS-FLI1 and can be further potentiated in combination with irinotecan. The net result was complete inhibition of EWS-FLI1 activity *in vivo*, sustained suppression of xenograft growth, and replacement of the xenografts with benign fat. Together, the results identify a novel EWS-FLI1 inhibitor and an approach to targeting fusion transcription factors based on the activation of wild-type functions of one of the fusion partners.

## Materials and Methods

### Cell culture

TC32, TC71, EW8, A673, RH30, and RD cells were all obtained from Dr. Lee Helman (NCI, Bethesda, MD), TC252 cells were a gift from Dr. Tim Triche (The Saban Research Hospital, Children's Hospital of Los Angeles, Los Angeles, CA), and MCF7 cells were a gift from Dr. P. Steeg (NCI, Bethesda, MD). A2058 cells were purchased from ATCC. All cell lines were routinely screened to confirm mycoplasma-negative status and to confirm the identity of the cells by short tandem repeat (STR) profiling (DDC Medical). The most recent STR testing was on November 30, 2014, for all the cells except A2058, which was tested on February 12, 2016. EWS-FLI1 expression was confirmed by RT-PCR. Cells were grown at 37°C with 5% CO<sub>2</sub>. RPMI1640 (Gibco) was supplemented with 10% FBS (Gemini Bio Products), 2 mmol/L L-glutamine, and 100 U/mL and 100 µg/mL penicillin and streptomycin, respectively (Gibco).

### Confocal microscopy

TC32 cells were incubated with compound for 6 hours in a Nunc Lab-Tek II Chamber Slide (Thermo Scientific), fixed in 4% paraformaldehyde in PBS, washed, lysed in 0.1% Triton X-100, and blocked in 10% goat serum (all in PBS). The cells were incubated with primary antibody (18 hours), secondary antibody (1 hour), and tertiary antibody for 30 minutes with washes in between, followed by mounting in ProLong Gold with DAPI (Life Technologies; primary antibodies: nucleolin, Abcam, 1:1,000; HA-tag, Abcam, 1:500; γH2AX, Millipore, 1:1,000; FLI1, Abcam, 1:100; secondary antibodies: biotin anti-mouse IgG, Vector Laboratories, 1:1,000; and tertiary antibodies: Strep-635, Life Technologies, 1:400; FITC-rabbit, Millipore, 1:200). All images were obtained with standardized settings on a Zeiss 510 confocal microscope. For BODIPY images, TC32 cells were treated as indicated. One hour prior to fixation in 4% paraformaldehyde, BODIPY 493/503 (Invitrogen) and Hoechst 33342 (Invitrogen) were added to the culture medium. The cells were washed and imaged.

### Cell proliferation assays

Cell viability IC<sub>50</sub>s were determined by nonlinear regression (GraphPad Prism) as the average of three independent experiments using standard MTS assay CellTiter 96 (Promega) following 48-hour incubation with drug as described previously (10). Real-time proliferation assays were performed on the Incucyte Zoom as described previously (11).

### Luciferase assays

Stable cell lines containing an EWS-FLI1-driven NR0B1 luciferase or constitutively active cytomegalovirus (CMV) control were incubated with drug in opaque 96-well plates (BD Falcon) for 8 hours (10). Cells were lysed in 100 µL of Steady-Glo (Promega), and bioluminescence was measured on a BioTek plate reader.

### Quantitative RT-PCR

TC32 or TC71 cells ( $3 \times 10^5$ ) were incubated with drug in 6-well plates (BD Falcon). RNA was collected using the RNeasy Kit (Qiagen) and immediately reverse transcribed using a High-Capacity Reverse Transcriptase Kit (Life Technologies) at 25°C for 10 minutes, 37°C for 120 minutes, and 85°C for 10 minutes. We subsequently PCR amplified 100 ng of cDNA, 2× SYBR Green (Bio-Rad), and the following program: 95°C for 10 minutes, 95°C for 15 seconds, 55°C for 15 seconds, and 72°C for 1 minute, for 40 cycles. Expression was determined from three independent experiments relative to GAPDH and solvent control using standard  $\Delta\Delta C_t$  methods. Primers sequences can be found in Supplementary Table S1. All PCR products were validated by gel electrophoresis, followed by standard Sanger sequencing (see Supplementary Fig. S1A and S1B for validation of NR0B1). Heatmaps were created using R v 3.2.2 (R Foundation for Statistical Computing) and comprise  $\Delta\Delta C_t$  scores truncated between -3 and 3 to prevent very large scores from oversaturating the color gradient.

### Western blotting

We incubated  $1.5 \times 10^6$  TC32 and TC71 cells with drug in 10-cm<sup>2</sup> dishes, scraped into cold PBS, washed in PBS, and lysed in 4% LDS lysis buffer. Following dilution of detergent, the protein was quantitated using the bicinchoninic colorimetric assay (Pierce, Thermo-Scientific). Thirty micrograms of total protein was resolved on a NuPage 4% to 12% Bis-Tris gradient gel (Invitrogen) in 1× NuPage MOPS SDS Running Buffer (Invitrogen) and transferred to nitrocellulose using 1× Tris/Glycine/SDS Buffer (Bio-Rad) supplemented with 20% methanol at 4°C overnight at 20 V. The membranes were subsequently blocked in 5% milk in TBS-T and probed with Abcam (FLI1, NR0B1, and GAPDH) or Cell Signaling Technology (EZH2 and ID2) antibodies.

### Xenograft experiments

TC71 or TC32 cells ( $2 \times 10^6$ ) were injected intramuscularly in the gastrocnemius of female 4- to 6-week-old female homozygous nude mice (CrI; Nu-Foxm1<sup>Nu</sup>; Harlan Laboratories, SL) and established to a minimum diameter of 0.5 cm. Four cohorts of 12 mice were treated with vehicle, lurbinectedin (0.18 mg/kg i.v.; TC32 days 0, 7; TC71 days 0, 7, 14), irinotecan (5 mg/kg i.p.; TC32 days 3, 10; TC71 days; 1 to 3, 8 to 10; 15 to 17), or the combination (same dose route and schedule as the individual tumor types). Tumor volume was measured three times per week and determined using the equation  $(D \times d^2)/6 \times 3.14$  (where D is the maximum diameter and d is the minimum diameter). Tissue was collected and fixed in 10% formalin. Mice were sacrificed when the tumor diameter reached 2 cm in any dimension. All experiments were performed in accordance with the guidelines and regulation of, and approved by, the animal care and use committee (PharmaMar). Investigators were not blinded to the treatment groups.

### Tissue staining

Paraffin-embedded tissue was sectioned into 5- $\mu$ m sections and mounted on Colomark Plus Charged Slides. Antigen retrieval was performed in Ventana CC1 or manually for immunofluorescence using citrate buffer (Dako). Following blocking, the tissue was incubated with NR0B1 primary (Abcam, 1:50), washed, and then incubated with secondary antibody (anti-rabbit Cy5 conjugated, Life Technologies).

### Oil Red O staining

TC32 cells were plated and treated in Nunc Lab-Tek II Chamber Slides (Thermo Scientific). Cells were washed with PBS, fixed for 30 minutes, and then washed with distilled water. Cells were incubated with isopropanol for 3 minutes and a working solution [filtered 3:2 Oil Red O (Sigma) to deionized water] of Oil Red O for 10 minutes. After aspirating the Oil Red O solution, the slides were briefly stained with hematoxylin solution (Sigma) and imaged using an Aperio scanning microscope (Leica).

### Immunofluorescence and IHC

Paraffin-embedded tissue was sectioned into 5- $\mu$ m sections and mounted on Colomark Plus Charged Slides. Antigen retrieval was performed on Ventana Discovery Automated Stainer. Immunofluorescence staining was performed using NR0B1 primary (Abcam, 1:300), Ventana Ultramap Rb HRP, and Ventana Discovery Cy5 amplification. IHC was performed using Ki67 (Spring Bioscience, 1:100) and cleaved caspase-3 (Cell Signaling Technology, 1:400) primary antibodies, Ventana Ultramap rb HRP and Ventana Chromomap DAB.

### Immunofluorescence quantitation

Fluorescent images were acquired at  $\times 20$  magnification using the PE Vectra automated multispectral slide imager. Fluorescence was quantitated using Inform software. Standard settings were used across all treatments for image acquisition and quantitation.

### RNA sequencing

RNA was extracted from three biological replicates for each experimental time point, and samples were submitted for  $1 \times 75$  bp sequencing on the Illumina NextSeq 500 at the Van Andel Research Institute (Grand Rapids, MI). Sequencing libraries were prepared using the Illumina TruSeq HT Kit. Read quality was assessed using FASTQC v. 0.11.3 and aligned to the hg19 genome using Subread v. 1.4.3. (12) with default parameters. Raw read counts to known exons were obtained using FeatureCounts v 1.4.3 using strand-specific read counting. Counts per million were calculated and log<sub>2</sub> transformed using voom (13). Transformation and differential expression analyses were conducted using the limma package v 3.28.7 in R (14) and are available (SRA accession: SRP080099). The EWS-FLI1 gene signature consists of all genes in common from two data sets, a meta-analysis and a list of differentially expressed genes obtained by expression profiling following silencing of EWS-FLI1 in five cell lines (3, 15). Genes induced (116) or repressed (50) by EWS-FLI1 were identified (Supplementary Table S2). Significance testing for enrichment of EWS-FLI1-induced or -repressed gene signatures from differentially expressed genes were performed using a hypergeometric test with the phyper function implemented in the R stats package (v 3.3.0; <https://cran.r-project.org/>). Heatmaps were generated using either the aheatmap function implemented in the NMF

package (v 0.20.6) or the pheatmap package (v 1.0.8) in R (v 3.3.0).

## Results

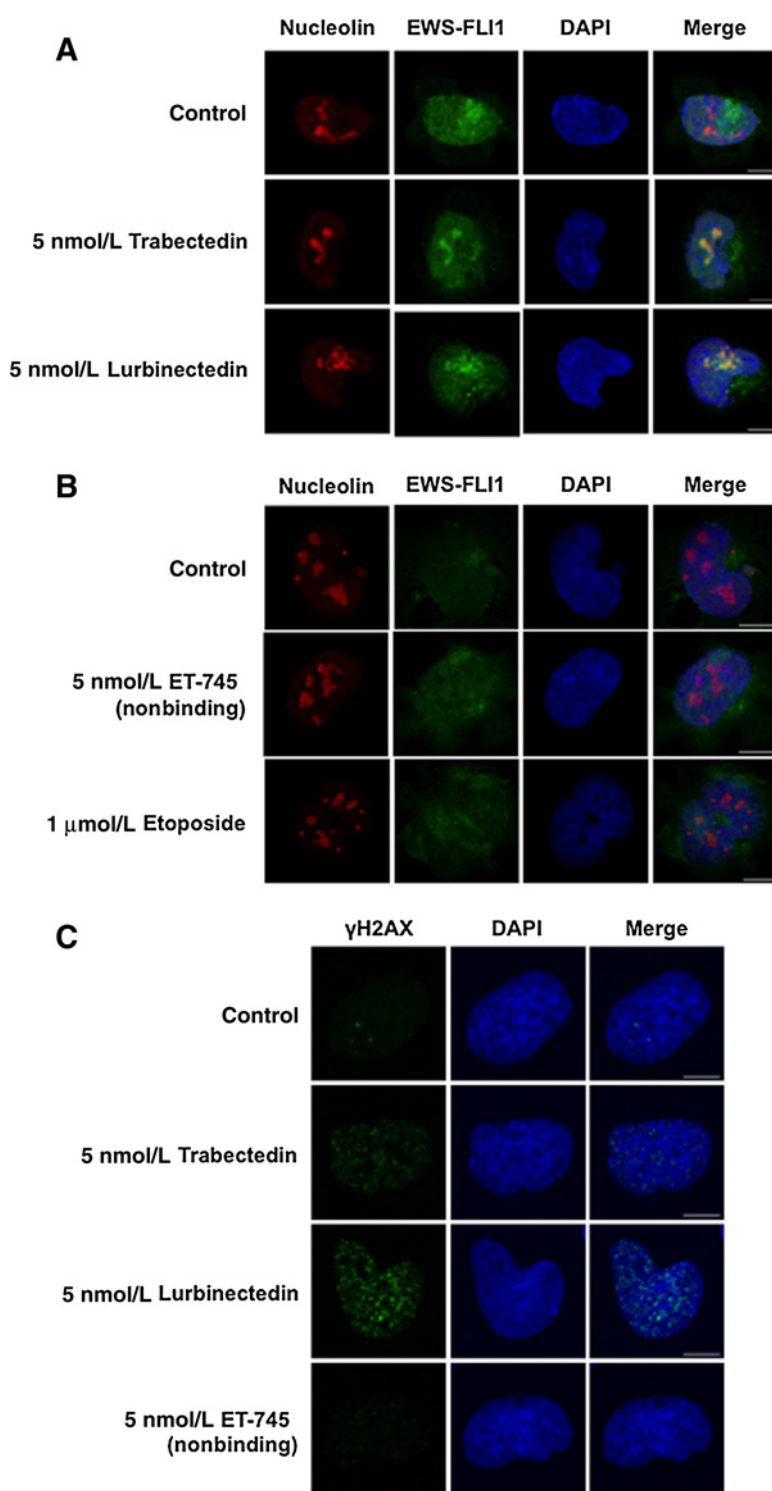
We have previously shown that trabectedin treatment leads to the induction of DNA damage and suppression of the EWS-FLI1 gene signature without globally suppressing transcription (9). This led to the paradoxical characterization of the drug as a DNA-damaging but molecularly targeted agent (16, 17). Therefore, we reasoned that the DNA damage induced by the drug may lead to a specific cellular response that poisons EWS-FLI1-directed transcription.

Treatment of TC32 Ewing sarcoma cells with 5 nmol/L of trabectedin caused EWS-FLI1 to redistribute within the nucleus and colocalize with the nucleolus marker nucleolin (Fig. 1A). This effect was observed with either an HA-tagged EWS-FLI1 or a FLI1 antibody against the c-terminus of EWS-FLI1 (FLI1 is not expressed in these cells; Supplementary Fig. S2). In addition, this effect required drug-induced DNA damage and binding, as a non-DNA binding trabectedin analogue, ET-745, did not result in the redistribution of EWS-FLI1 (Fig. 1B) or accumulation of phosphorylated H2AX foci (Fig. 1C). Finally, this effect was not the result of generalized DNA damage, as relocalization did not occur with high concentration of the topoisomerase II inhibitor etoposide (Fig. 1B).

To assess the clinical applicability of the effect, we evaluated the degree of relocalization that occurred at 2.5 nmol/L, a concentration that approximates the  $C_{max}$  in the phase II study in Ewing sarcoma patients, and we found minimal relocalization (Supplementary Fig. S3A). Therefore, we evaluated a second-generation trabectedin analogue, lurbinectedin, which is known to have an improved pharmacokinetic profile and to accumulate in serum to levels greater than 170 ng/mL (215 nmol/L; ref. 18). Lurbinectedin redistributed EWS-FLI1 to the nucleolus to the same degree as trabectedin at 5 nmol/L (Fig. 1A).

To show that the mislocalization of EWS-FLI1 induced by lurbinectedin leads to a loss in EWS-FLI1 activity, we demonstrated that 5 nmol/L lurbinectedin suppressed an EWS-FLI1-driven (NR0B1) luciferase reporter to 42% of control (Fig. 2A; ref. 10). This suppression paralleled the effect of 5 nmol/L trabectedin (46% of control). In contrast, only modest suppression (77% of control) of a constitutively active CMV reporter was found at the identical concentration and time (Fig. 2A). Importantly, these concentrations were exactly the values that cause redistribution of EWS-FLI1 within the nucleus.

Next, we showed that suppression of EWS-FLI1 extended to other EWS-FLI1 targets. As there is no established gene signature of EWS-FLI1, we selected EWS-FLI1 target genes from numerous published studies, used siRNAs targeting the breakpoint of EWS-FLI1 to selectively silence the fusion protein, and confirmed the suppression of these targets (see Supplementary Table S3 for evidence; refs. 3, 10, 15, 19–28). All of the EWS-FLI1-induced targets were repressed, and the selected repressed targets were induced with siRNA silencing of EWS-FLI1 (Fig. 2B, left). Next, we showed that treatment of TC32 Ewing sarcoma cells with 5 nmol/L lurbinectedin reproduced the effect of siRNA silencing of EWS-FLI1, causing all of the EWS-FLI1-induced genes to be suppressed and all of the EWS-FLI1-repressed targets to be induced (Fig. 2B, right). To validate these results, we also evaluated the effect of drug treatment on

**Figure 1.**

EWS-FLI1 changes localization upon trabectedin or lurbinectedin treatment. **A**, single-cell imaging of HA-tagged TC32 cells treated with 5 nmol/L trabectedin or lurbinectedin for 6 hours shows EWS-FLI1 (green) localization into the nucleolus (red). DAPI (blue) was used as a nuclear stain. **B**, single-cell imaging of HA-tagged TC32 cells treated with ET-745 or etoposide shows a lack of EWS-FLI1 nucleolar localization. **C**, single-cell imaging of TC32 cells treated with 5 nmol/L trabectedin, lurbinectedin, or ET-745 for 6 hours shows the appearance of  $\gamma$ H2AX (green) foci. DAPI (blue) was used as a counterstain. Scale bars, 10  $\mu$ m.

four additional targets used by other investigators as markers of EWS-FLI1 activity, *LOX*, *BCL11B*, *STEAP1*, and *PRKCB* (29–32). All of the induced targets were suppressed, while *LOX* showed minimal change with treatment (Supplementary Fig. S4A).

To show that these effects are not restricted to these selected targets, we evaluated the effect of lurbinectedin treatment on the gene signature of EWS-FLI1 using RNA sequencing. We found that

treatment of lurbinectedin for 6 or 12 hours led to a marked suppression (93/116; 80%) of genes normally induced by EWS-FLI1 (Fig. 3A). Furthermore, the EWS-FLI1-induced gene signature was significantly enriched ( $P = 0.006$ ) within the differentially expressed genes (adjusted  $P < 0.05$ ), suggesting that drug treatment disrupts aberrant EWS-FLI1 induction of gene expression. Interestingly, the gene signature of repressed targets did not

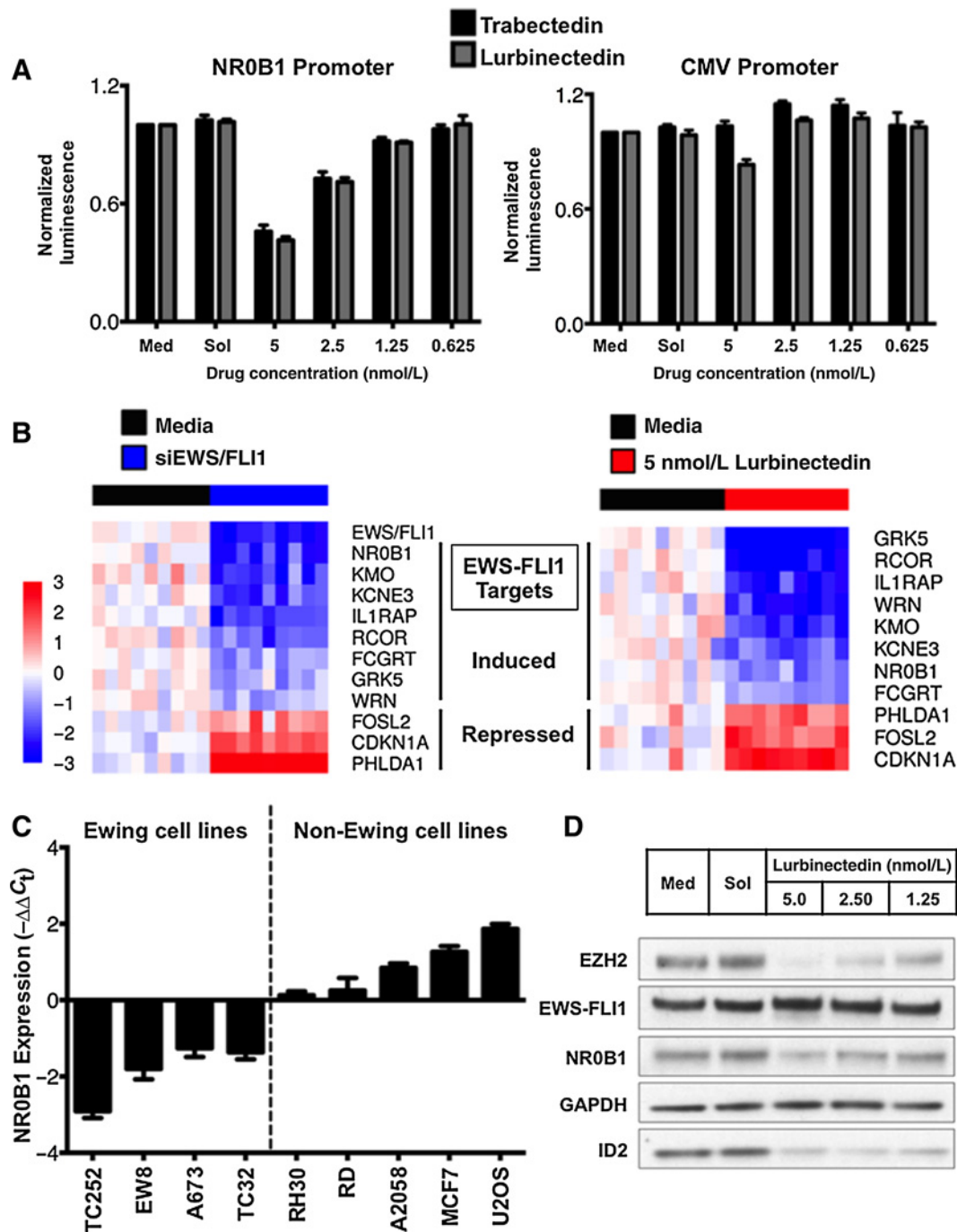


**Figure 2.**

Lurbinectedin treatment mimicked the response to EWS/FLI1 knockdown and trabectedin treatment (black bars) or lurbinectedin (gray bars) on an *NR0B1* promoter luciferase or CMV-driven reporter. Cells were treated for 8 hours at the indicated concentrations, and MTS assays were performed in parallel to ensure that the suppressive effects were not a consequence of cell death. **B**, heatmap showing a similar effect of siRNA-mediated silencing of EWS-FLI1 (left) and 12-hour 5 nmol/L lurbinectedin treatment (right). **C**, suppression of *NR0B1* was restricted to Ewing sarcoma cell lines, as shown by the effect of 5 nmol/L lurbinectedin treatment for 12 hours in a panel of cell lines. **D**, lurbinectedin treatment for 18 hours suppressed the expression of the EWS-FLI1 downstream target proteins *NR0B1*, *EZH2*, and *ID2* but not EWS-FLI1 itself or GAPDH as measured by Western blot analysis.

show clear induction of all of the targets, although targets that appear on multiple EWS-FLI1-repressed target gene lists were induced by lurbinectedin treatment (Supplementary Fig. S4B;

targets highlighted in the figure; refs. 3, 15). Finally, to exclude a general repression of transcription as the cause for reversal of the gene signature, we also examined the effect of lurbinectedin

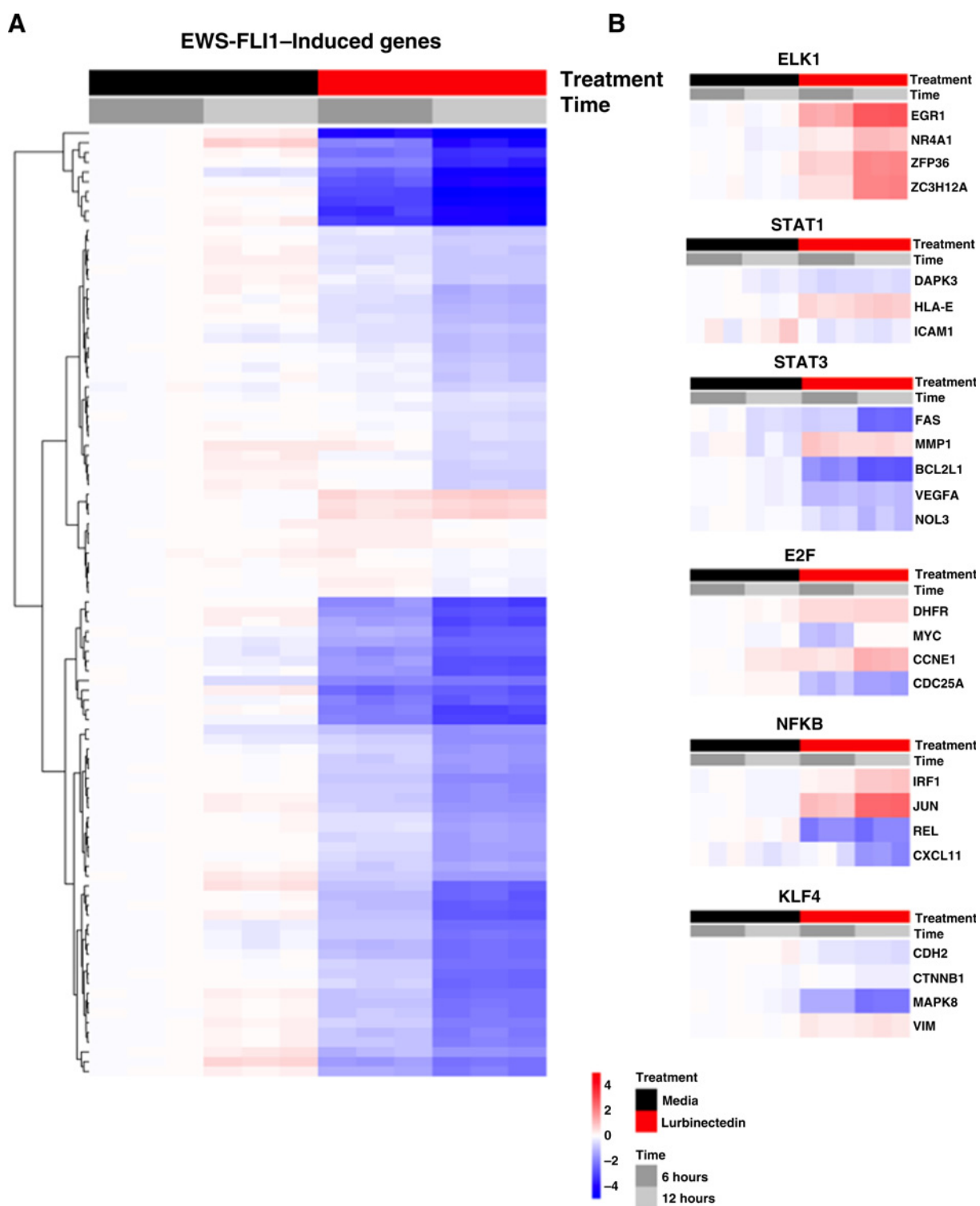


**Figure 3.** Lurbinectedin suppresses EWS-FLI1 activity, but not the activity of other transcription factors. **A**, heatmap showing the majority of EWS-FLI1-induced genes are suppressed by lurbinectedin treatment at 6 and 12 hours relative to the media control using RNA-seq. Med, media; sol, solvent. Genes shown are differentially expressed (adjusted  $P < 0.05$ ), and the scale represents  $\log_2$  fold-changes relative to the mean of the comparator (6-hour media). **B**, heatmaps of additional and related (ELK1) transcription factors suggesting that lurbinectedin is not acting as a general transcription factor inhibitor.

Downloaded from <http://aacrjournals.org/cancerres/article-pdf/76/22/6657/12738001/6657.pdf> by guest on 26 August 2022

treatment on expression of well-characterized target genes that are driven by transcription factors other than EWS-FLI1, including a family member of FLI1, ELK1 (Fig. 3B; refs. 33–39). Notably, ELK1 target genes are induced in the presence of drug, suggesting that lurbinectedin may not be acting as a general transcription factor inhibitor. We demonstrate a mixed effect of lurbinectedin on the expression of target genes of these transcription factors (Fig. 3B).

As further evidence that this reflects an EWS-FLI1-specific effect, we evaluated the effect of lurbinectedin treatment on *NR0B1* expression in a panel of cell lines. *NR0B1* is a well-established EWS-FLI1 target gene whose expression is driven by binding of the fusion protein to a GGAA microsatellite contained within the gene's promoter (21). Both wild-type FLI1 and EWS-FLI1 are capable of binding this microsatellite, but only EWS-FLI1 can activate transcription (40). Consistent with this, in four different Ewing sarcoma cell lines (TC32, EW8, TC252, and A673), lurbinectedin repressed *NR0B1* expression as measured by qRT-PCR. In contrast, treatment of a panel of non-EWS-FLI1-containing control cell lines led to either no change in expression of *NR0B1* (RH30 and RD lines) or induction of *NR0B1* mRNA expression (A2058, MCF7, and U2OS; Fig. 2C).

Finally, we showed that the suppression of EWS-FLI1 activity extended to the protein level by demonstrating the effect of lurbinectedin treatment on the important EWS-FLI1 target genes *NR0B1*, *ID2*, and *EZH2* (Fig. 2D). The treatment resulted in the marked suppression of proliferation and a subnanomolar  $IC_{50}$  that was similar to that of trabectedin (Supplementary Fig. S4C). The pharmacokinetic profile of lurbinectedin improves the likelihood of achieving this effect in patients.

We next evaluated the ability of irinotecan or its active metabolite, SN38, to synergize with lurbinectedin (23). SN38 enhances the transcriptional repression of EWS-FLI1 by trabectedin (23). This loss of EWS-FLI1 activity leads to a loss of expression of the EWS-FLI1 downstream target *WRN*, establishing a hypersensitivity to the DNA-damaging properties of camptothecin (41–43). Importantly, the combination of trabectedin and irinotecan has shown evidence of activity in a treatment-refractory Ewing sarcoma patient in the clinic (44).

Similar to the case with trabectedin, treatment of TC32 Ewing sarcoma cells with a relatively low dose (2.5 nmol/L) of lurbinectedin caused minimal but evident EWS-FLI1 relocalization (Supplementary Fig. S2) and marginally suppressed expression of the EWS-FLI1 target genes *NR0B1*, *ID2*, and *EZH2* by Western blot analysis (Fig. 3A, lane 3). However, when lurbinectedin was combined with SN38, we observed a marked suppression and a virtual elimination of expression of the EWS-FLI1 target genes (Fig. 4A, lanes 7–9). Importantly, the effect of SN38 on EWS-FLI1-driven transcription was not due to cooperative relocalization of EWS-FLI1 to the nucleolus, as there was no effect on the nuclear distribution of EWS-FLI1 with SN38 treatment (Fig. 4B). Furthermore, the suppression of EWS-FLI1 activity by lurbinectedin was accompanied by a dose-dependent suppression of *WRN* helicase expression (Fig. 4C), which established the hypersensitivity to the DNA-damaging properties of SN38 and the synergy of the two agents (Fig. 4D; Table 1; refs. 41–43).

To test the combination of lurbinectedin and irinotecan *in vivo*, we evaluated two different xenograft models of Ewing sarcoma, TC71 and TC32. Both cohorts were treated with lurbinectedin at

0.18 mg/kg i.v. on days 0, 7 (TC32) or 0, 7, 14 (TC71). TC71 mice were treated with irinotecan (5 mg/kg) on days 1 to 3, 8 to 10, and 15 to 17; TC32 mice received irinotecan on days 3 and 10. Both single-agent therapies delayed tumor growth, and the combination therapy led to a sustained regression of tumors from both xenografts (Supplementary Fig. S5) that translated into an improvement in the fraction of animals surviving (Fig. 5A). It is notable that 30% of the mice bearing the TC32 xenograft and 70% of mice bearing the TC71 xenograft treated with the combination therapy did not reach a 2-cm diameter until well after 100 days, even though the mice were showing no evidence of toxicity and therapy was stopped on day 10 (TC32) or 17 (TC71). This effect was rooted in the suppression of EWS-FLI1 because treatment of these mice with lurbinectedin alone suppressed *NR0B1* expression as measured by a novel immunofluorescent assay (Fig. 5B, control staining and quantitation shown in Supplementary Fig. S6A).

It is notable that the mice experienced very little toxicity and had a marginal reduction in weight gain relative to control animals (Supplementary Fig. S5, bottom). It is likely that this marginal toxicity is due to the fact that the therapy was extremely effective and therefore required only a short duration of treatment (Fig. 5A and Supplementary Fig. S5).

To explain the persistence of the effect after cessation of therapy, we evaluated the effect of drug treatment on the morphology of the xenograft. We found that tumors treated with the combination showed a time-dependent, nearly complete replacement of the tissue with benign fat (Fig. 5C). Within the tumor sections, there were focal zones that appeared to be actively differentiating (Fig. 5D). The fat in these areas were human in origin and stained positive with ALU-*ish*, a marker of human DNA or a human-specific mitochondrial antibody (Fig. 5D). These areas were also positive for Ki67 but not cleaved caspase-3 (Supplementary Fig. S6B). Nevertheless, the staining for the human markers faded away from these regions, consistent with known remodeling that occurs with human fat xenografts in immunocompromised mice (Supplementary Fig. S6C; ref. 45). Indeed, this effect presents a challenge to breast cancer xenograft studies (45). This result is consistent with the differentiation of at least a portion of the tumor into benign fat, as well as loss of EWS-FLI1 activity that is known to repress differentiation, particularly for EWS-FLI1-repressed targets (3, 6).

Finally, to ensure that the differentiation phenotype was a result of drug treatment and not a result of the mouse microenvironment, we examined the ability of Ewing sarcoma cells to differentiate *in vitro*. While continuous exposure to lurbinectedin led to the induction of fat differentiation genes, *CEBPA* and *PPARG*, over 48 hours, the net effect was cytotoxicity with very few viable cells evident at 48 hours (Fig. 6A and B). However, brief exposures to drug led to sustained effects on tumor proliferation, with as little as 30 minutes of exposure to lurbinectedin (Fig. 6A). Indeed, 60 minutes of exposure to lurbinectedin led to the long-term suppression of proliferation that was accompanied by the robust induction of the fat differentiation genes *CEBPA* and *PPARG* as well as evidence of accumulation of neutral lipid in the Ewing sarcoma cells as measured by two different neutral lipid stains, Oil RedO and BODIPY (Fig. 6B–D). In essence, these effects recapitulate the results seen with siRNA silencing of EWS-FLI1 that has been previously reported as well as the differentiation we observed here in animal models (7). Importantly, the *in vitro*

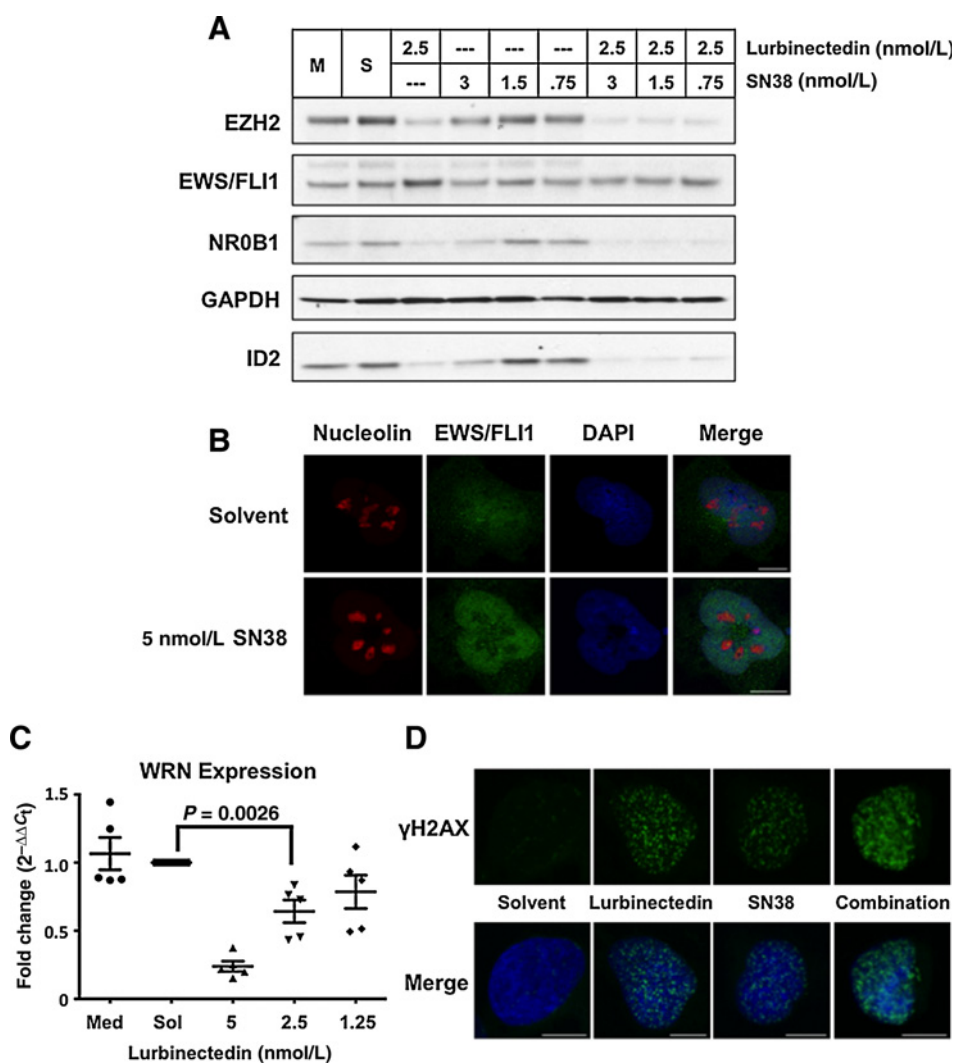


**Figure 4.**

Lurbinectedin synergized with SN38 to poison EWS/FLI1 activity and induced DNA damage. **A**, Western blot analysis of TC32 cells after 18 hours of treatment with either lurbinectedin alone, SN38 alone, or the combination at the indicated concentrations. M, media; S, solvent. **B**, confocal microscopy of nucleolin (red) and EWS/FLI1 (green) in response to 5 nmol/L SN38 treatment after 6 hours. DAPI (blue) staining of the nucleus. **C**, quantitative PCR analysis of WRN mRNA expression in TC32 cells upon 12-hour treatment with lurbinectedin at the indicated concentrations. **D**, single-cell confocal microscopy showing  $\gamma$ H2AX (green) foci upon 12-hour treatment with 5 nmol/L of lurbinectedin, 5 nmol/L of SN38, or the combination. DAPI (blue) staining of the nucleus. *P* value was determined using a two-sided Student *t* test. Scale bars, 10  $\mu$ m.

exposures with washout are more reflective of the exposures seen in the mouse, although higher concentration and longer exposures should be attainable in patients consistent with the overall goals of the study (18, 46).

## Discussion

In this report, we describe a novel approach to target oncogenic fusion proteins. We exploit the inherent competition between the oncogenic properties of the fusion protein and the retained wild-type functions of one of the fusion partners. By activating the DDR of EWSR1, we are able to reposition EWS-FLI1 within the nucleus to suppress its activity. In the process, we provide evidence that a DNA-binding and DNA-

damaging agent can serve as a targeted agent. In addition, we characterize a novel mechanism of tumor differentiation and show evidence for this process both *in vitro* and *in vivo*.

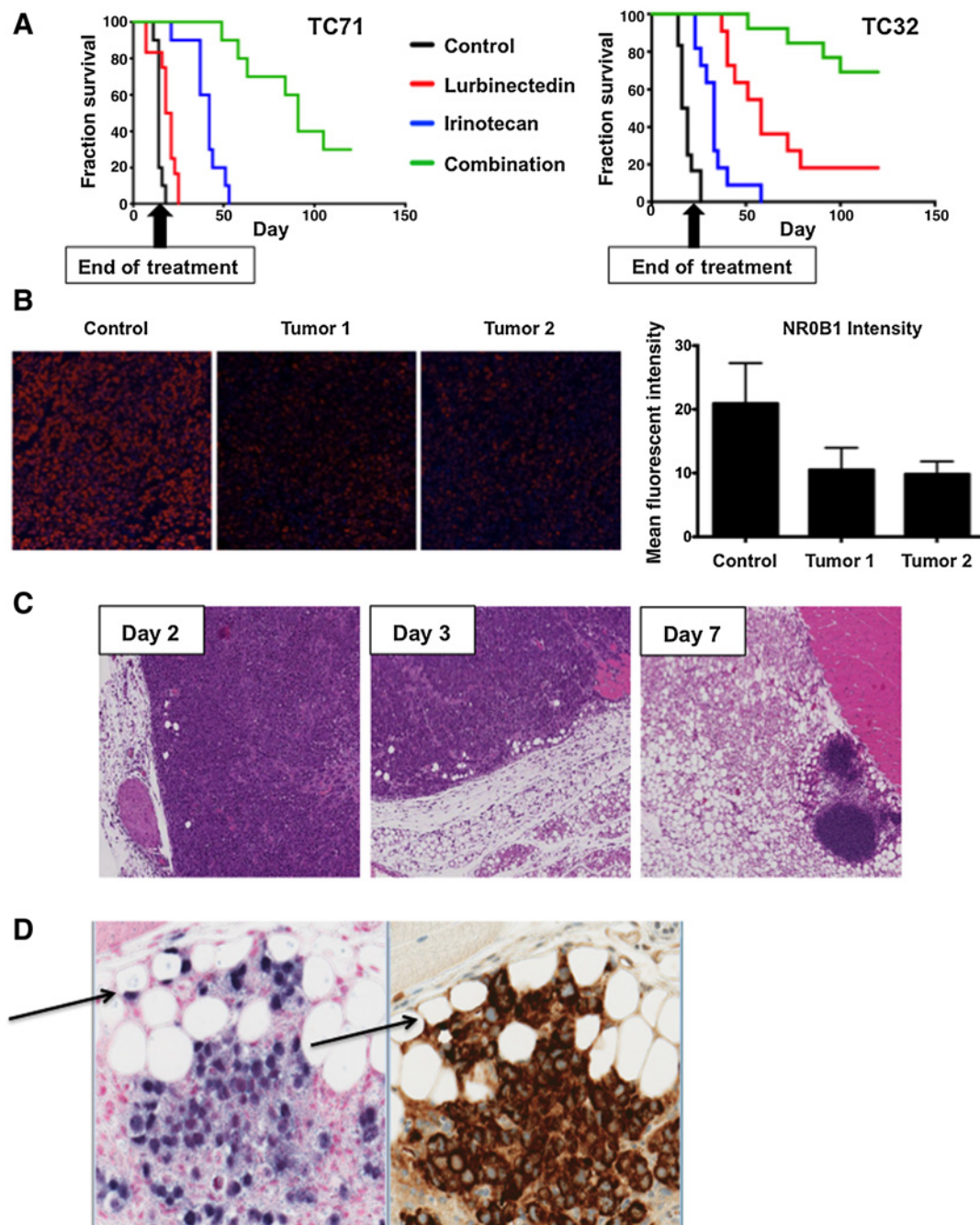
The mechanism described in this study may explain the activity of trabectedin against Ewing sarcoma in the clinic. There was originally widespread interest in trabectedin for this disease because of a complete response in a treatment-refractory Ewing sarcoma patient in the phase I pediatric study (47). However, the follow-up phase II study in Ewing sarcoma was negative (48). The main difference between the studies (beyond the study design and goals) was a change in schedule in the phase II that led to a substantially lower  $C_{max}$  in the patient's serum. In our study, the levels of drug achieved in the phase II study (around 2.5 nmol/L) caused minimal redistribution of

**Table 1.** Combination index values

	Experimental points			Median effect equation	
	$2 \times IC_{50}$	$IC_{50}$	$0.5 \times IC_{50}$	$ED_{50}$	$ED_{75}$
Trabectedin & SN38	$1.03 \pm 0.07$	$0.67 \pm 0.03$	$1.04 \pm 0.24$	$0.55 \pm 0.25$	$0.82 \pm 0.23$
Lurbinectedin & SN38	$0.93 \pm 0.10$	$0.63 \pm 0.03$	$1.10 \pm 0.24$	$0.67 \pm 0.09$	$0.81 \pm 0.09$

NOTE: CI values show synergy between lurbinectedin and irinotecan.  $CI < 1$  = synergy;  $CI = 1$  is additive;  $CI > 1$  = antagonism.



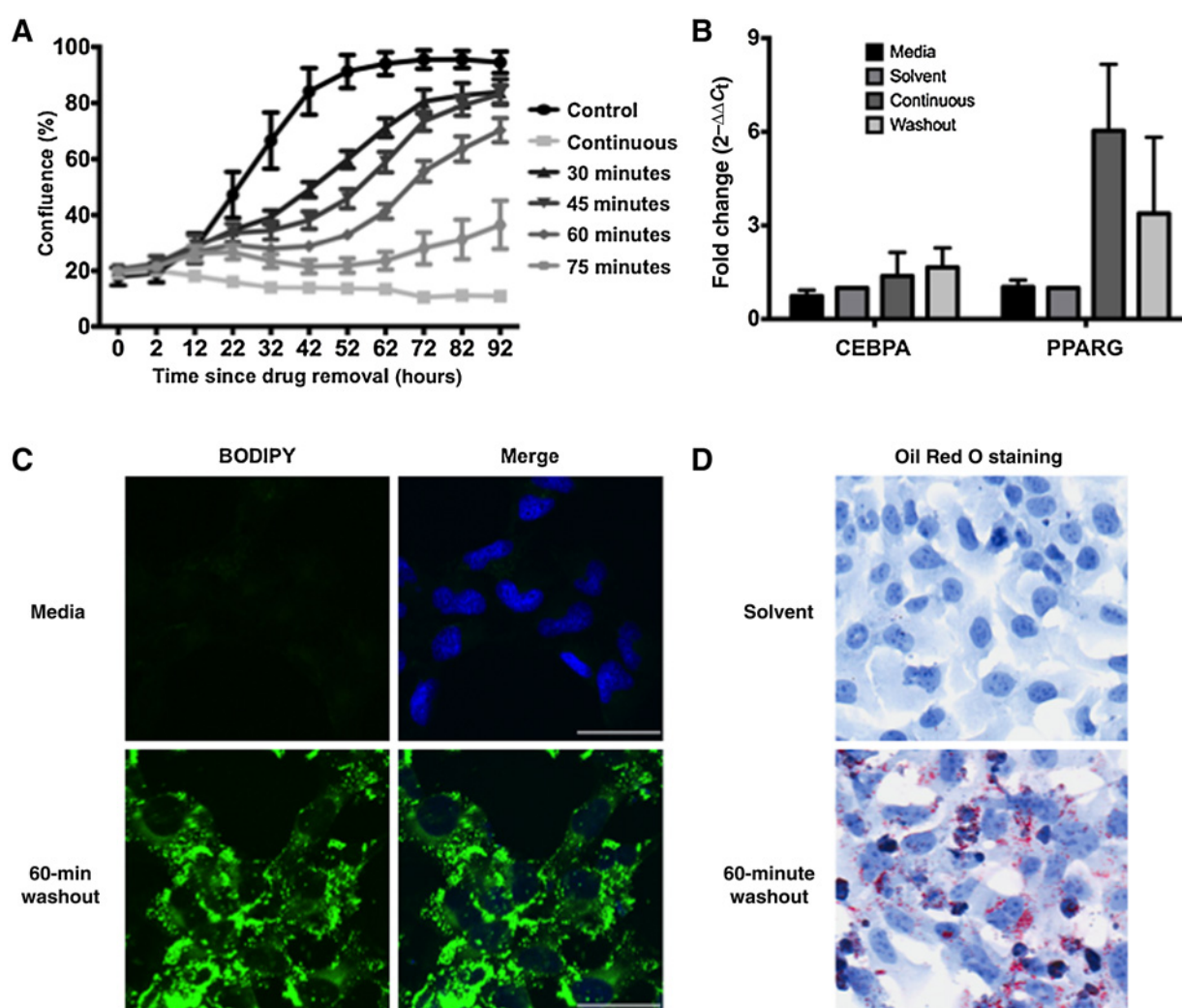


**Figure 5.**

The combination of lurbinectedin and irinotecan suppressed Ewing sarcoma xenograft growth and EWS-FLI1 activity *in vivo*. **A**, survival curves for mice bearing TC71 (left) or TC32 (right) xenografts. Both cohorts were treated with lurbinectedin on days 0 and 7. TC32 mice were treated with irinotecan on days 3 and 10, whereas TC71 mice received an additional dose of lurbinectedin on day 14 and irinotecan on days 1 to 3, 8 to 10, and 15 to 17. All groups survived significantly longer than control (all  $P < 0.0001$ ).  $P$  value was determined using Cox proportional hazards regression. **B**, left, immunofluorescence images from xenograft tissue showing NR0B1 staining (red) in the control and lurbinectedin cohorts at day 3. Right, quantification of the immunofluorescence imaging on the left. Images were obtained at  $\times 20$  magnification. **C**, hematoxylin and eosin staining showing gradual differentiation of TC71 tumor into fat in mice; samples collected on days 2, 3, and 7 of treatment with both irinotecan and lurbinectedin. **D**, section of xenograft containing adipocytes of human origin (arrows). Left, stains, ALUish DNA probes for human-specific ALU repeat elements at  $\times 20$ ; right, human-specific mitochondrial surface stain.

EWS-FLI1 and marginal suppression of EWS-FLI1 activity. In contrast, the phase I serum levels ( $>10$  nmol/L) would be sufficient to cause this redistribution of EWS-FLI1 and suppress-

ion of activity, perhaps accounting for the response to the drug seen in the clinic. Therefore, it is possible that the activity of trabectedin seen in the phase I study may be reproduced in the

**Figure 6.**

Transient lurbinectedin treatment induces adipogenic differentiation. **A**, TC32 growth curves as measured by percent confluence. TC32 cells were treated with 10 nmol/L lurbinectedin for the indicated time period followed by 4 days in regular RPMI media. **B**, treatment of TC32 cells for 60 minutes with 10 nmol/L lurbinectedin induces expression of terminal adipogenic transcription factors, CEBPA and PPARG. **C**, confocal imaging of BODIPY dye comparing solvent with 10 nmol/L lurbinectedin washout. Images were taken 48 hours after the drug was removed from the media. BODIPY, neutral lipid dye; Hoechst, DNA stain. **D**, Oil Red O staining comparing solvent and 10 nmol/L lurbinectedin washout. Images were taken 48 hours after drug was removed from the media. Images were taken at  $\times 20$  magnification. Scale bars, 50  $\mu\text{m}$ .

phase II setting if the drug is given as a 3-hour infusion. This likelihood of response would be increased by combining the drug with the potentiator, low-dose irinotecan, as has been recently reported in the clinic (44).

Alternatively, the suppression of EWS-FLI1 could be improved by using a second-generation compound, lurbinectedin, which has an improved pharmacokinetics profile, making the redistribution of EWS-FLI1 more easily attainable in patients. In this study, we show the redistribution of EWS-FLI1 occurs with lurbinectedin at 5 to 10 nmol/L while the  $C_{\text{max}}$  of this drug is around 182.2 ng/mL or  $>200$  nmol/L (18). Furthermore, we show that irinotecan potentiates lurbinectedin-mediated EWS-FLI1 suppression. Finally, we show that lurbinectedin sensitizes cells to irinotecan-mediated DNA damage, leading to marked synergy between the two agents. It is notable that combination therapies

involving irinotecan have shown good activity in the clinic and therefore are commonly used as part of salvage regimens for the disease (49). It is possible that these irinotecan-based combination therapies can be improved by centering the synergy around the therapeutic suppression of EWS-FLI1, where lurbinectedin sensitizes to irinotecan and irinotecan, in turn, potentiates lurbinectedin.

Together, these results provide a novel approach to the targeting of oncogenic transcription factors and a new EWS-FLI1-directed therapy for Ewing sarcoma.

#### Disclosure of Potential Conflicts of Interest

M.J. Guillen Navarro is a team leader at PharmaMar. C.M. Galmarini is the senior manager at PharmaMar SA. P.M. Aviles is the manager at PharmaMar. No potential conflicts of interest were disclosed by the other authors.

## Disclaimer

The content is solely the responsibility of the authors and does not necessarily represent the official views of the NIH.

## Authors' Contributions

**Conception and design:** M.L. Harlow, M.J. Guillen Navarro, M. D'Incalci, C.M. Galmarini, P.M. Aviles, P.J. Grohar

**Development of methodology:** M.L. Harlow, S.M. Kitchen-Goosen, M. D'Incalci, L. Turner, P.J. Grohar

**Acquisition of data (provided animals, acquired and managed patients, provided facilities, etc.):** M.L. Harlow, J. Roland, M.K. Easton, S.M. Kitchen-Goosen, E.A. Boguslawski, P.J. Grohar

**Analysis and interpretation of data (e.g., statistical analysis, biostatistics, computational analysis):** M.L. Harlow, J. Roland, S.M. Kitchen-Goosen, E.A. Boguslawski, Z.B. Madaj, B.K. Johnson, M.J. Bowman, M.E. Winn, G. Hostetter, P.J. Grohar

**Writing, review, and/or revision of the manuscript:** M.L. Harlow, M.J. Guillen Navarro, Z.B. Madaj, B.K. Johnson, M.J. Bowman, M.E. Winn, C.M. Galmarini, P.M. Aviles, P.J. Grohar

**Administrative, technical, or material support (i.e., reporting or organizing data, constructing databases):** M.L. Harlow, G. Hostetter, P.J. Grohar

**Study supervision:** M.L. Harlow, P.J. Grohar

**Other (provided data):** N. Maloney

## References

- Delattre O, Zucman J, Plougastel B, Desmaze C, Melot T, Peter M, et al. Gene fusion with an ETS DNA-binding domain caused by chromosome translocation in human tumours. *Nature* 1992;359:162–5.
- Maksimenko A, Malvy C. Oncogene-targeted antisense oligonucleotides for the treatment of Ewing sarcoma. *Expert Opin Ther Targets* 2005; 9:825–30.
- Kauer M, Ban J, Kofler R, Walker B, Davis S, Meltzer P, et al. A molecular function map of Ewing's sarcoma. *PLoS One* 2009;4:e5415.
- Li KK, Lee KA. Transcriptional activation by the Ewing's sarcoma (EWS) oncogene can be cis-repressed by the EWS RNA-binding domain. *J Biol Chem* 2000;275:23053–8.
- Alex D, Lee KA. RGG-boxes of the EWS oncoprotein repress a range of transcriptional activation domains. *Nucleic Acids Res* 2005;33:1323–31.
- Torchia EC, Jaishankar S, Baker SJ. Ewing tumor fusion proteins block the differentiation of pluripotent marrow stromal cells. *Cancer Res* 2003; 63:3464–8.
- Tirode F, Laud-Duval K, Prieur A, Delorme B, Charbord P, Delattre O. Mesenchymal stem cell features of Ewing tumors. *Cancer Cell* 2007;11: 421–9.
- Paronetto MP, Minana B, Valcarcel J. The Ewing sarcoma protein regulates DNA damage-induced alternative splicing. *Mol Cell* 2011;43:353–68.
- Grohar PJ, Griffin LB, Yeung C, Chen QR, Pommier Y, Khanna C, et al. Ecteinascidin 743 interferes with the activity of EWS-FLI1 in Ewing sarcoma cells. *Neoplasia* 2011;13:145–53.
- Grohar PJ, Woldemichael GM, Griffin LB, Mendoza A, Chen QR, Yeung C, et al. Identification of an inhibitor of the EWS-FLI1 oncogenic transcription factor by high-throughput screening. *J Natl Cancer Inst* 2011;103:962–78.
- Osgood CL, Maloney N, Kidd CG, Kitchen-Goosen S, Segars L, Gebregiorgis M, et al. Identification of mithramycin analogues with improved targeting of the EWS-FLI1 transcription factor. *Clin Cancer Res* 2016; 22:4105–18.
- Liao Y, Smyth GK, Shi W. The Subread aligner: fast, accurate and scalable read mapping by seed-and-vote. *Nucleic Acids Res* 2013;41:e108.
- Law CW, Chen Y, Shi W, Smyth GK. voom: Precision weights unlock linear model analysis tools for RNA-seq read counts. *Genome Biol* 2014;15:R29.
- Ritchie ME, Phipson B, Wu D, Hu Y, Law CW, Shi W, et al. limma powers differential expression analyses for RNA-sequencing and microarray studies. *Nucleic Acids Res* 2015;43:e47.
- Hancock JD, Lessnick SL. A transcriptional profiling meta-analysis reveals a core EWS-FLI gene expression signature. *Cell Cycle* 2008;7:250–6.
- Forni C, Minuzzo M, Virdis E, Tamborini E, Simone M, Tavecchio M, et al. Trabectedin (ET-743) promotes differentiation in myxoid liposarcoma tumors. *Mol Cancer Ther* 2009;8:449–57.
- D'Incalci M, Galmarini CM. A review of trabectedin (ET-743): a unique mechanism of action. *Mol Cancer Ther* 2010;9:2157–63.
- Elez ME, Taberero J, Geary D, Macarulla T, Kang SP, Kahatt C, et al. First-in-human phase I study of lurbinectedin (PM01183) in patients with advanced solid tumors. *Clin Cancer Res* 2014;20:2205–14.
- Dohjima T, Lee NS, Li H, Ohno T, Rossi JJ. Small interfering RNAs expressed from a Pol III promoter suppress the EWS/FLI-1 transcript in an Ewing sarcoma cell line. *Mol Ther* 2003;7:811–6.
- Wei GH, Badis G, Berger MF, Kivioja T, Palin K, Enge M, et al. Genome-wide analysis of ETS-family DNA-binding in vitro and in vivo. *EMBO J* 2010;29:2147–60.
- Gangwal K, Sankar S, Hollenhorst PC, Kinsey M, Haroldsen SC, Shah AA, et al. Microsatellites as EWS/FLI response elements in Ewing's sarcoma. *Proc Natl Acad Sci U S A* 2008;105:10149–54.
- Patel M, Simon JM, Iglesia MD, Wu SB, McFadden AW, Lieb JD, et al. Tumor-specific retargeting of an oncogenic transcription factor chimera results in dysregulation of chromatin and transcription. *Genome Res* 2012;22:259–70.
- Grohar PJ, Segars LE, Yeung C, Pommier Y, D'Incalci M, Mendoza A, et al. Dual targeting of EWS-FLI1 activity and the associated DNA damage response with trabectedin and SN38 synergistically inhibits Ewing sarcoma cell growth. *Clin Cancer Res* 2014;20:1190–203.
- Mendiola M, Carrillo J, Garcia E, Lalli E, Hernandez T, de Alava E, et al. The orphan nuclear receptor DAX1 is up-regulated by the EWS/FLI1 oncoprotein and is highly expressed in Ewing tumors. *Int J Cancer* 2006;118:1381–9.
- Kinsey M, Smith R, Iyer AK, McCabe ER, Lessnick SL. EWS/FLI and its downstream target NR0B1 interact directly to modulate transcription and oncogenesis in Ewing's sarcoma. *Cancer Res* 2009;69:9047–55.
- Tong DL, Boockch DJ, Dhondalay GK, Lemette C, Ball GR. Artificial neural network inference (ANNI): a study on gene-gene interaction for biomarkers in childhood sarcomas. *PLoS One* 2014;9:e102483.
- Nakatani F, Tanaka K, Sakimura R, Matsumoto Y, Matsunobu T, Li X, et al. Identification of p21WAF1/CIP1 as a direct target of EWS-FLI1 oncogenic fusion protein. *J Biol Chem* 2003;278:15105–15.
- Boro A, Prete K, Rechfeld F, Thalhammer V, Oesch S, Wachtel M, et al. Small-molecule screen identifies modulators of EWS/FLI1 target gene expression and cell survival in Ewing's sarcoma. *Int J Cancer* 2012;131: 2153–64.
- Sankar S, Bell R, Stephens B, Zhuo R, Sharma S, Bearss DJ, et al. Mechanism and relevance of EWS/FLI-mediated transcriptional repression in Ewing sarcoma. *Oncogene* 2013;32:5089–100.
- Wiles ET, Lui-Sargent B, Bell R, Lessnick SL. BCL11B is up-regulated by EWS/FLI and contributes to the transformed phenotype in Ewing sarcoma. *PLoS One* 2013;8:e59369.

## Acknowledgments

The authors would like to thank David Nadziejka for technical editing of the manuscript.

## Grant Support

Research reported in this article was supported by the NCI of the NIH under award number R01CA188314 (P.J. Grohar). Funding to develop the immunofluorescent assay was provided by the Alex's Lemonade Stand Reach Award (P.J. Grohar). Additional internal funds were provided by the Vanderbilt University (Department of Pediatrics) and the Lily's Garden Foundation (P.J. Grohar). Internal funding from the Van Andel Institute helped support this study (P.J. Grohar). Funding supporting M. D'Incalci's research program is provided by the Italian Association for Cancer Research (AIRC).

The costs of publication of this article were defrayed in part by the payment of page charges. This article must therefore be hereby marked *advertisement* in accordance with 18 U.S.C. Section 1734 solely to indicate this fact.

Received February 26, 2016; revised August 31, 2016; accepted September 5, 2016; published OnlineFirst October 3, 2016.

31. Grunewald TG, Diebold I, Esposito I, Plehm S, Hauer K, Thiel U, et al. STEAP1 is associated with the invasive and oxidative stress phenotype of Ewing tumors. *Mol Cancer Res* 2012;10:52–65.
32. Surdez D, Benetkiewicz M, Perrin V, Han ZY, Pierron C, Ballet S, et al. Targeting the EWSR1-FLI1 oncogene-induced protein kinase PKC-beta abolishes ewing sarcoma growth. *Cancer Res* 2012;72:4494–503.
33. Kasza A. Signal-dependent Elk-1 target genes involved in transcript processing and cell migration. *Biochim Biophys Acta* 2013;1829:1026–33.
34. Bhinge AA, Kim J, Euskirchen GM, Snyder M, Iyer VR. Mapping the chromosomal targets of STAT1 by Sequence Tag Analysis of Genomic Enrichment (STAGE). *Genome Res* 2007;17:910–6.
35. Regis G, Pensa S, Boselli D, Novelli F, Poli V. Ups and downs: the STAT1: STAT3 seesaw of Interferon and gp130 receptor signalling. *Semin Cell Dev Biol* 2008;19:351–9.
36. Carpenter RL, Lo HW. STAT3 target genes relevant to human cancers. *Cancers* 2014;6:897–925.
37. Bracken AP, Ciro M, Cocito A, Helin K. E2F target genes: unraveling the biology. *Trends Biochem Sci* 2004;29:409–17.
38. Pahl HL. Activators and target genes of Rel/NF-kappaB transcription factors. *Oncogene* 1999;18:6853–66.
39. Tiwari N, Meyer-Schaller N, Arnold P, Antoniadis H, Pachkov M, van Nimwegen E, et al. Klf4 is a transcriptional regulator of genes critical for EMT, including Jnk1 (Mapk8). *PLoS One* 2013;8:e57329.
40. Gangwal K, Close D, Enriquez CA, Hill CP, Lessnick SL. Emergent properties of EWS/FLI regulation via GGAA microsatellites in Ewing's Sarcoma. *Genes Cancer* 2010;1:177–87.
41. Poot M, Gollahon KA, Rabinovitch PS. Werner syndrome lymphoblastoid cells are sensitive to camptothecin-induced apoptosis in S-phase. *Hum Genet* 1999;104:10–4.
42. Lebel M, Leder P. A deletion within the murine Werner syndrome helicase induces sensitivity to inhibitors of topoisomerase and loss of cellular proliferative capacity. *Proc Natl Acad Sci U S A* 1998;95:13097–102.
43. Pichierri P, Franchitto A, Mosesso P, Palitti F. Werner's syndrome cell lines are hypersensitive to camptothecin-induced chromosomal damage. *Mutat Res* 2000;456:45–57.
44. Tancredi R, Zambelli A, DaPrada GA, Fregoni V, Pavesi L, Riccardi A, et al. Targeting the EWS-FLI1 transcription factor in Ewing sarcoma. *Cancer Chemother Pharmacol* 2015;75:1317–20.
45. Proia DA, Kuperwasser C. Reconstruction of human mammary tissues in a mouse model. *Nat Protoc* 2006;1:206–14.
46. Pemice T, Bishop AG, Guillen MJ, Cuevas C, Aviles P. Development of a liquid chromatography/tandem mass spectrometry assay for the quantification of PM01183 (lurbinectedin), a novel antineoplastic agent, in mouse, rat, dog, Cynomolgus monkey and mini-pig plasma. *J Pharm Biomed Anal* 2016;123:37–41.
47. Lau L, Supko JG, Blaney S, Hershon L, Seibel N, Krailo M, et al. A phase I and pharmacokinetic study of ecteinascidin-743 (Yondelis) in children with refractory solid tumors. A Children's Oncology Group study. *Clin Cancer Res* 2005;11:672–7.
48. Baruchel S, Pappo A, Krailo M, Baker KS, Wu B, Villaluna D, et al. A phase 2 trial of trabectedin in children with recurrent rhabdomyosarcoma, Ewing sarcoma and non-rhabdomyosarcoma soft tissue sarcomas: a report from the Children's Oncology Group. *Eur J Cancer* 2012;48:579–85.
49. Wagner L. Camptothecin-based regimens for treatment of ewing sarcoma: past studies and future directions. *Sarcoma* 2011;2011:957957.